american physiological society

JNP JOURNAL OF NEUROPHYSIOLOGY

*J Neurophysiol* 132: 1857–1866, 2024.
*First published October 30, 2024; doi:10.1152/jn.00298.2024*

RESEARCH ARTICLE

*Control of Movement*

# Head rotations follow those of a truncated Fick gimbal during an auditory-guided visual search task

**Glen McLachlan,[1] Pedro Lladó,[2] and Herbert Peremans[1]**

[1]*Active Perception Lab, Department of Engineering Management, University of Antwerp, Belgium and* [2]*Acoustics Lab, Department of Information and Communication Engineering, Aalto University, Espoo, Finland*

## Abstract

Recent interest in dynamic sound localization models has created a need to better understand the head movements made by humans. Previous studies have shown that static head positions and small oscillations of the head obey Donders' law: for each facing direction there is one unique three-dimensional orientation. It is unclear whether this same constraint applies to audiovisual localization, where head movement is unrestricted and subjects may rotate their heads depending on the available auditory information. In an auditory-guided visual search task, human subjects were instructed to localize an audiovisual target within a field of visual distractors in the frontal hemisphere. During this task, head and torso movements were monitored with a motion capture system. Head rotations were found to follow Donders' law during search tasks. Individual differences were present in the amount of roll that subjects deployed, though there was no statistically significant improvement in model performance when including these individual differences in a gimbal model. The roll component of head rotation could therefore be predicted with a truncated Fick gimbal, which consists of a pitch axis nested within a yaw axis. This led to a reduction from three to two degrees of freedom when modeling head movement during localization tasks.

**NEW & NOTEWORTHY** Understanding how humans utilize head movements during sound localization is crucial for the advancement of auditory perception models and improvement of practical applications like hearing aids and virtual reality systems. By analyzing head motion data from an auditory-guided visual search task, we concluded that findings from earlier studies on head movement can be generalized to audiovisual localization and, from this, proposed a simple model for head rotation that reduced the number of degrees of freedom.

*audiovisual localization; Donders' law; Fick gimbal; head movement*

## INTRODUCTION

Sound localization performance improves when listeners are able to move their heads during stimulus presentation. Changes in interaural cues as a result of head movement help resolve front-back confusions and can, in certain situations, improve elevation estimation (1–7).

Traditionally, experiments and models of human sound localization have mainly focused on passive localization, where the head remains stationary. However, new available technologies in head tracking and virtual reality have led to a growing interest in understanding how head movements affect sound localization performance (8). A few models exist that consider the dynamic position of the head during sound localization (9, 10), though this remains a relatively new area of study and introduces a number of new challenges in auditory modeling. First, it raises the question of how acoustic and sensorimotor information are combined. Second, the incoming information needs to be integrated over time. Third, a separate movement model must be defined to simulate head rotation. In this article we focus on addressing the latter challenge.

Models of head motion have been proposed in the past with various levels of complexity. There are models that consider rotation (11, 12), translation (13), or acceleration patterns (14). Movement also seems to depend highly on the individual (15). Furthermore, experiments that also investigated unrestricted and natural head movement found that

Correspondence: G. McLachlan (glen.mclachlan@uantwerpen.be).
Submitted 15 August 2024 / Revised 7 October 2024 / Accepted 8 October 2024

movement is task dependent (12, 16), so a model for one task may not be applicable to another. In the context of sound localization, it is possible that humans move their heads to optimize the acoustic information that they receive, which may lead to its own unique head movement behavior (17, 18).

The arguments above make it difficult, though important, to find general rules of head motion that may simplify a movement model. A common example of such simplifications is the assumption that humans generally move their heads according to Donders' law, i.e., the head does not make use of all three degrees of freedom when rotating (19–21). Rather, for any direction of the head, its rotation around its direction is unique. In other words, the amount of roll (i.e., torsion) is not controlled separately; instead it is a function of the amount of yaw (i.e., horizontal) and pitch (i.e., vertical) rotation (11, 13). Note that humans are anatomically capable of executing independent roll rotations but Donders' law implies that, in practice, humans do not utilize this additional degree of freedom.

The goal of the present study is to investigate head movement behavior by collecting head (and torso) motion data during an auditory-guided visual search task. More specifically, we wish to answer two subsequent questions: *1*) do the head movements in this task follow Donders' law and *2*) how can we best model this? The results of this study can then be used to integrate a more realistic movement model into existing active sound localization models.

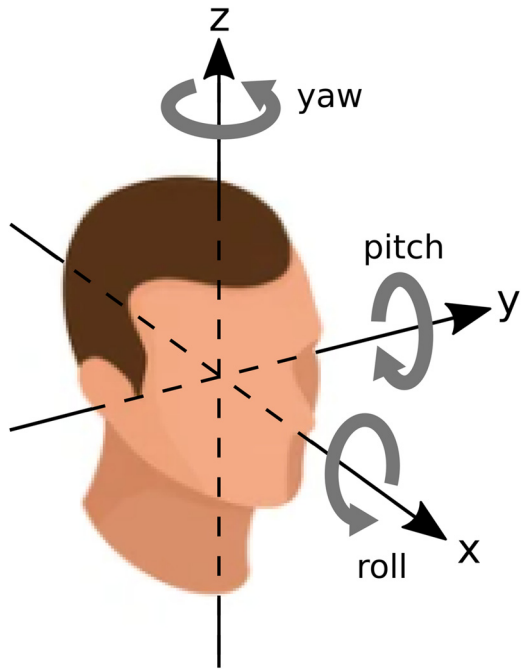


**Figure 1.** Visualization of 3-dimensional axes and corresponding positive rotations.

## METHODS

### Coordinate and Rotation Conventions in Three Dimensions

All axes and rotations described in this article follow the right-hand rule and are expressed in the global coordinate system, with the axes fixed to the world. The positive $x$-axis points forward, with positive roll rotations toward the right shoulder. The positive $y$-axis points to the left, with positive pitch rotations downward. The positive $z$-axis points upward, with positive yaw rotations toward the left. The coordinate system and the directions of rotation are illustrated in Fig. 1.

The orientation of an object in a three-dimensional space with respect to a fixed coordinate system can be described by a set of three rotations around three principal axes, the Euler angles.

If $\theta$ is the rotation angle around a single axis, then rotation over the spatial $x$-axis, i.e., roll, is defined as:

$$R_x(\theta_x) = \begin{pmatrix} 1 & 0 & 0 \\ 0 & \cos(\theta_x) & -\sin(\theta_x) \\ 0 & \sin(\theta_x) & \cos(\theta_x) \end{pmatrix} \quad (1)$$

Rotation over the spatial $y$-axis, i.e., pitch, is defined as:

$$R_y(\theta_y) = \begin{pmatrix} \cos(\theta_y) & 0 & \sin(\theta_y) \\ 0 & 1 & 0 \\ -\sin(\theta_y) & 0 & \cos(\theta_y) \end{pmatrix} \quad (2)$$

Rotation over the spatial $z$-axis, i.e., yaw, is defined as:

$$R_z(\theta_z) = \begin{pmatrix} \cos(\theta_z) & -\sin(\theta_z) & 0 \\ \sin(\theta_z) & \cos(\theta_z) & 0 \\ 0 & 0 & 1 \end{pmatrix} \quad (3)$$

The rotation matrix to obtain the final orientation can be expressed by a successive multiplication of the three single-axis rotation operators. This can be done in any order, but this will result in different final orientations, so it is also important to define the order of rotations. In this article we follow the Fick convention, which defines $R$ as a rotation over the $x$-axis, then the $y$-axis, and then the $z$-axis, using world-fixed rotation axes.

$$R = R_z \cdot R_y \cdot R_x \quad (4)$$

We can also express rotation matrix $R$ as a vector $\mathbf{r}$, which can bring the object from the reference orientation to the orientation of interest by just one rotation around a single axis. This representation has been used in several studies investigating head and eye movements (12, 13, 22).

Rotation vector $\mathbf{r}$ with components $(r_x, r_y, r_z)^T$ is defined as (22):

$$\mathbf{r} = \frac{1}{1 + R_{11} + R_{22} + R_{33}} \times \begin{pmatrix} R_{32} - R_{23} \\ R_{13} - R_{31} \\ R_{21} - R_{12} \end{pmatrix} \quad (5)$$

where $R_{ij}$ are the indices of rotation matrix $R$, where $i$ is the row and $j$ is the column. The length of $\mathbf{r}$ is a function of the angle of rotation $\alpha$ around the vector $|\mathbf{r}| = \tan(\alpha/2)$, and the direction of the rotation axis coincides with that of $\mathbf{r}$, again using the right-hand rule for the sense of rotation.

### Models for Head Rotation

According to Donders' law, the rotation vectors of a head rotation in any direction should fit on a second-order twisted surface (23):

$$r_x = a_1 + a_2 r_y + a_3 r_z + a_4 r_y^2 + a_5 r_y r_z + a_6 r_z^2 \quad (6)$$

where $a_1$ adjusts the surface offset, $a_2$ and $a_3$ adjust the surface orientation, $a_4$ and $a_6$ yield a parabolic curvature, and $a_5$ allows for the surface to twist.

By examining the roll, pitch, and yaw components of the rotation vector, it was inferred that the constraints on the head during natural movement resemble a specific form of Donders' law, following the rotations of a truncated Fick gimbal (with no roll axis) (12, 16, 24). Here the yaw axis of rotation is fixed relative to the trunk and can change the direction of the supported pitch axis (25). Thus, the roll component of the rotation vector ($r_x$) in such a system is not controlled independently but depends on the eccentricity of oblique facing directions. The truncated Fick gimbal is illustrated in Fig. 2*A*.

Kunin et al. (12) further extended the truncated Fick gimbal system by utilizing a coefficient, $k$, that reflects the ratio of the angles by which the first and second pitch axes rotate: $k\theta_2 = (1 - k)\theta_1$. This system is referred to as the $k$-gimbal model (see Fig. 2*C*). This model provides a mathematical and biomechanical explanation for the types of roll rotation made as a result of yaw and pitch rotation, resulting in the following relationship (12):

$$r_x = r_z \cdot \tan(2k \cdot \tan^{-1} r_y - \tan^{-1} r_y) + r_{x0} \quad (7)$$

where $r_{x0}$ is the amount of roll offset. If $k = 0$, then the model represents a truncated Fick gimbal; if $k = 1$, then it represents a truncated Helmholtz gimbal (see Fig. 2).

### Apparatus

The subjective evaluation took place in the multichannel anechoic chamber "Wilska" at Aalto University's Acoustics Lab (Espoo, Finland). A total of 20 Genelec 8331A coaxial loudspeakers were arranged in the frontal hemisphere, positioned 2.04 m from the center (see Fig. 3). These loudspeakers were placed at four distinct elevations. On the horizontal plane, seven loudspeakers were evenly spaced with an angular separation of 30° in azimuth. On the planes with ±30° in elevation, five loudspeakers were evenly spaced with an angular separation of 45°. On the plane with an elevation of 60°, three loudspeakers were evenly spaced with an angular separation of 90°. In one of the experimental conditions, sources at azimuth 90° and −90° were excluded to prevent unnecessary neck strain for the subjects (represented in Fig. 3 as empty circles). See *Experimental Conditions* for detailed information about the experimental conditions.

A 2 × 2 LED matrix (with a 15-mm center-to-center spacing) was installed directly in front of each loudspeaker, serving as a visual target for the search task. The target loudspeaker's LED matrix always displayed an even number of illuminated red LEDs (either 2 or 4, randomly determined for each trial). Nontarget loudspeakers displayed an odd number of illuminated LEDs (1 or 3, randomly determined for each loudspeaker). The LED system was controlled by an Arduino UNO WiFi Rev2, interfaced with Max 8 via serial communication. An auditory stimulus synchronized with the visual target was emitted from the target loudspeaker to assist in locating the visual target. This sound stimulus consisted of pink noise with an onset ramp of 10 ms, as described in Method 3 of ANSI/ASA S3.71 (26), set at an A-weighted level of 65 dB SPL measured at the subject's position. The stimulus continued until the subject responded. The room lights were dimmed to aid the visual search task.

The head and torso movements were tracked with Motive software and six OptiTrack Prime 13W cameras at a sampling rate of 100 Hz. The origin of the world coordinates was calibrated at floor level beneath the chair in which the subjects were seated. The origin of the head tracker was calibrated for each individual separately, at the center of the head and slightly above eye level. Reflective markers were located on a hat and the torso of the subjects to track head and torso movements, respectively, which were grouped as rigid bodies in Motive to analyze these two body parts separately.

To control the participants' field of view in the experiment, pinhole goggles were constructed by taping off standard protective construction goggles. This left only a small rectangular aperture through which a single target could be seen at any given time, with a maximum width of 30°.

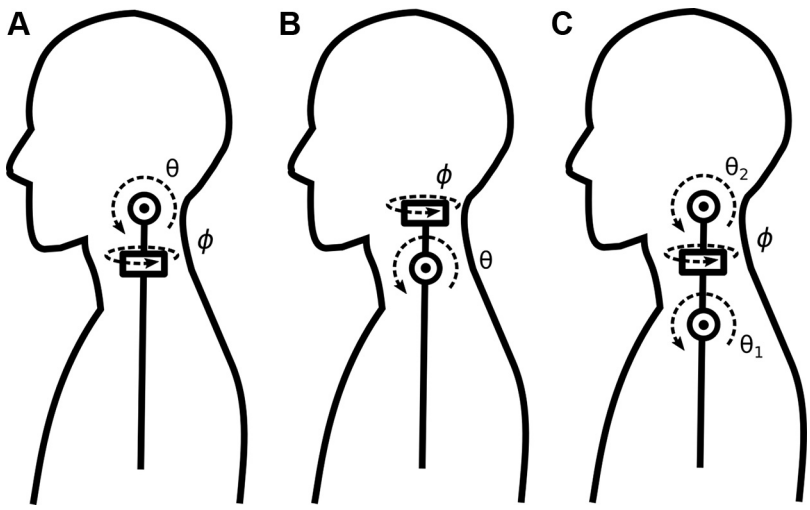


**Figure 2.** Truncated Fick gimbal (*A*), truncated Helmholtz gimbal (*B*), and *k*-gimbal model (*C*), where θ denotes a pitch rotation and ϕ denotes a yaw rotation. Note that the axes were visually separated for clarity; the models do not undergo any translation. The upper rotation axes are nested within the bottom axes, e.g., the truncated Fick gimbal is a pitch axis nested within a yaw axis.

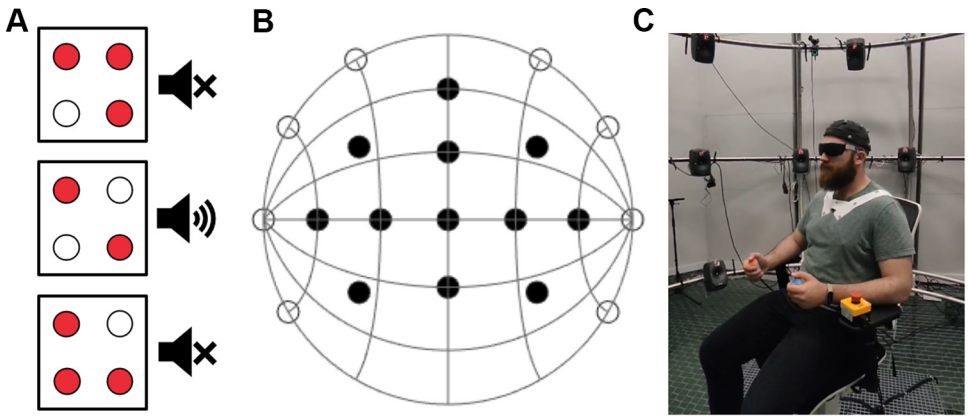


**Figure 3.** *A*: example of target and 2 distractor LED clusters. *B*: source direction distribution in the frontal hemisphere, used during the listening experiments. Empty circles were excluded in condition PG (pinhole goggles). *C*: photo of experimental setup, including pinhole goggles and head and shoulder reflectors for tracking.

### Experimental Conditions

Three movement conditions were tested, each intended to incentivize different modes of movement. In all conditions subjects were seated in a fixed chair with arm rests; hence the subjects' hips were fixed. In the first condition, subjects were instructed not to move the torso. We refer to this as the no torso (NT) condition. In the second condition, the subjects also could not move the torso, and, in addition, they wore pinhole goggles that blocked their peripheral vision. It was checked that the subject could not see more than one loudspeaker at a time with the pinhole goggles before the experiment started. This forced them to fully rotate their heads toward a source to see it, as opposed to merely rotating to bring it into their field of view. We refer to this as the pinhole goggles (PG) condition. In this PG condition, sources at azimuth 90° and −90° were excluded, to prevent unnecessary neck strain for the subjects. In the third condition, the subjects were free to move however they preferred from a seated position, including head and torso movements. We refer to this as the free (F) condition. No further instructions were given on how the head or body should be moved.

### Subjects

During a recruitment period from May 10th to May 19th, 2023, 17 Caucasian subjects (3 female, 14 male) were recruited from the staff at Aalto University for the experiment. Subjects provided written informed consent and reported normal hearing and no recent neck injuries. The age range of the subjects was between 19 and 34 yr. There was no financial compensation for participating in the experiment.

### Experimental Design

The localization task conducted here was inspired by the experimental design used in Bolia et al. (27), Simpson et al. (28), and Lladó et al. (29) and was adopted by the standard "Methods for measuring the effect of head-worn devices on directional sound localization in the horizontal plane" (26). The subject held two buttons, which were used to answer how many LEDs were activated at the target. Left (blue) indicated two, and right (red) indicated four.

At the start of each trial, the subject oriented their body and head straight forward facing the LED board at (0° azimuth, 0° elevation). A new trial was initiated by pressing the two buttons at the same time. The LEDs were activated on all loudspeakers. Simultaneously, an acoustic stimulus was played from the target direction. The subject then searched the field to localize the target. Once the target was identified, the subject had to press the appropriate button, according to the correct number of LEDs activated. The sound stimulus was presented until a response button was pressed. The head tracking for each trial began when the stimulus was presented and was terminated when the subject pressed the response button.

The order of conditions and source directions was randomized independently for each subject, and only one movement condition was tested within a single block of trials. Each source direction was presented a total of five times per block.

This experiment was performed under ethical approval for listening experimentation by the Research Ethics Committee of Aalto University.

### Postprocessing and Statistical Analyses

The tracker data were rotated and translated per subject by the median starting position of that subject, so that the resulting median starting orientation and translation of the center of the head was at zero along all world-centered axes for each subject.

Trials were omitted if they had unrealistic roll values larger than 50° or durations that exceeded 5 s or, in the case of NT and PG, had torso rotations that exceeded 5°. This resulted in 1 + 2 + 166 total omissions, respectively, out of 4,165 trials. This means that the majority of omissions were due to forbidden torso rotations. For the calculation of gimbal scores and $k$ values, data points were only considered for rotations larger than 6°.

As a statistical measure of the goodness of fit of the twisted surfaces to the obtained data, the $R^2$ is reported. The statistical significance between performance of the truncated Fick gimbal model and alternative model implementations was tested with two-tailed $t$ tests.

## RESULTS

### Maximum Rotations

We calculated the medians, upper and lower quartiles, and ranges of the minimum and maximum rotations made

over all trials. These results are plotted in Fig. 4, separated for the world-centered yaw, pitch, and roll axes and for all test conditions.

Unsurprisingly, the largest rotations were made around the yaw axis. The maximum yaw rotation was the same for conditions NT and PG, even though the maximum directions of the stimuli were not the same (see Fig. 3). When localizing sound, subjects will often rotate their heads toward the presented sounds, though they do not necessarily fully turn their heads to face the stimulus (30). The field of view then appeared to be responsible for a discrepancy of ~30° between the orientation of the head and the stimulus orientation.

Pitch rotation was asymmetrical: extension (negative pitch) reached larger angles than flexion (positive pitch). This is likely caused by the distribution of the stimuli, which omitted the lowest elevations (see Fig. 3). The maximum rotations for pitch were larger in condition PG. Again this is most likely because the restricted field of view forces the subject to (almost) fully rotate toward each source. In condition NT, subjects made almost no use of flexion.

The lowest rotations were seen around the roll axis. However, with maximum rotations up to 20°, the roll axis is still important to consider for potential acoustic cues, which can already be informative for rotations smaller than 10° (10).

There was very little difference between conditions NT and F. The maximum ranges were slightly larger for condition F, as were the lower and upper quartiles. However, the lower and upper quartiles of torso rotations were found to be smaller than 2°, indicating that very little use was made of the extra allowed freedom of movement. Thus, for the remainder of the article we focus on the results of conditions NT and PG, where no torso movements were allowed.

Together, these general results show that, without torso movement, the maximum ranges of head rotation are around 60° for yaw and pitch rotation and 20° for roll rotation.

Note that the obtained data contained significant variances in starting positions between subjects. This is a result of individual differences in what is considered a comfortable "resting" position for the head. For example, some subjects consistently rested their head at 10° or 20° below the calibrated zero-pitch orientation. Note that the plots in Fig. 4 show values after the median initial orientation over all trials was set to zero.

## Rotation Trajectories

The azimuth trajectories over time of all trials performed by all subjects are plotted in Fig. 5*A*. The same trajectories are plotted on a sphere in Fig. 5*B*, which provides pitch rotation information instead of time information. For both conditions, the target that elicited the maximum rotation size was selected; this was source direction (90, 60) for condition NT and (45, 30) for condition PG. The source directions are indicated with a red cross.

The shapes of the rotation trajectories were similar between subjects. In the time domain, trajectories consistently followed a sigmoid curve, with the maximum velocity halfway through the rotation. This pattern has also been observed in other studies (31, 32). Trajectories in condition PG had more consistent end points than when full vision was available. This is because the subjects were forced to fully rotate toward the location of the target to see it; this adds a factor of consistency between subjects. In condition NT, any end point that contains the target within the field of view is acceptable. The start points were more consistent for the same reason: it was easier to align the head to a straightforward direction, because the target at (0, 0) was only visible at this exact orientation.

## Twisted Surfaces

To test the viability of Donders' law, we fitted a surface to the rotation vectors of the data of each subject with a nonlinear least-squares solver in MATLAB lsqcurvefit. The procedure minimized the residual error $\epsilon$ for the fitted twisted surface:

$$r_x = a_1 + a_2 r_y + a_3 r_z + a_4 r_y^2 + a_5 r_y r_z + a_6 r_z^2 + \epsilon \qquad (8)$$

Figure 6 shows the trajectories of the rotation vectors for each trial and the fitted twisted surfaces to those trajectories for the subjects with the highest value, the median, and the lowest value of $a_5$, respectively; values for $a_5$ and $R^2$ are reported in the bottom right corner for each subject. The top row in Fig. 6 shows the results for condition NT ($a_5 = -0.50, -0.96, -1.80$); the bottom row shows the same results for condition PG ($a_5 = -0.41, -0.77, -1.14$).

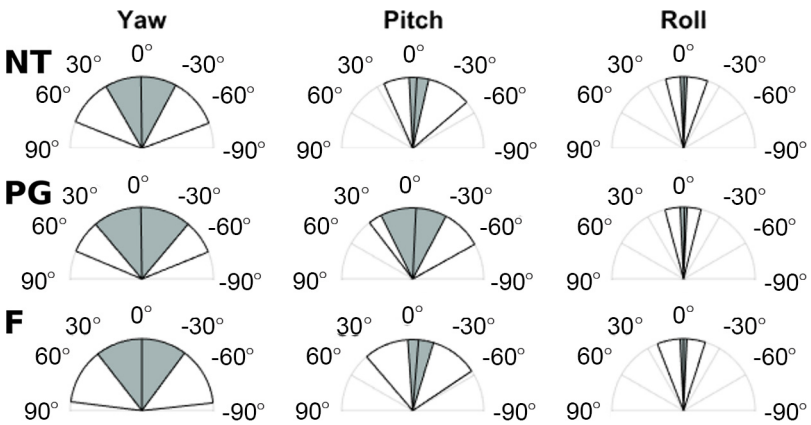


**Figure 4.** Median, upper and lower quartiles, and ranges of maximum rotations made over all trials. Results are separated for the world-centered yaw, pitch, and roll axes for movement conditions NT (no torso), PG (pinhole goggles), and F (free). Note that negative pitch is an upward rotation.

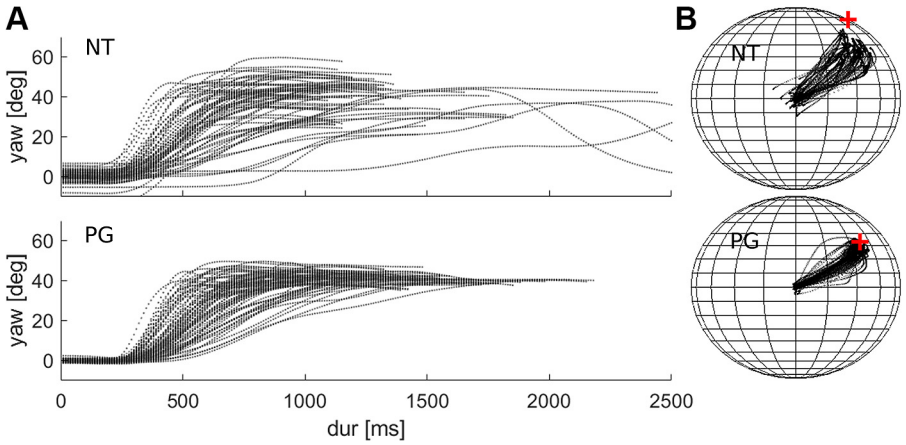


**Figure 5.** Trajectory plots of the head, for all trials toward the same target direction [no torso (NT): (90, 60), *top*; pinhole goggles (PG): (45, 30), *bottom*]. Distance between dots indicates a higher velocity. *A*: yaw trajectories plotted against time. *B*: trajectories plotted on a sphere. The red cross indicates the source direction.

Table 1 presents the means and standard deviations of the fitted twisted surface parameters for conditions NT and PG, alongside the results from an earlier study on head rotation, where subjects were instructed to rotate the head from a central position toward 12 targets on a circle in front of them, arranged like the hours on the face of a clock (13). The mean and standard deviation of $a_5$ (NT: $-1.062 \pm 0.321$, PG: $-0.794 \pm 0.171$) were similar to those found in the reference study ($-0.732 \pm 0.268$).

As a metric for the goodness of fit of the twisted surfaces we used the coefficient of determination, $R^2$. In Fig. 7 we report $R^2$ scores of the fitted twisted surfaces for conditions NT and PG. This was computed first with all parameters included, followed by individually excluding each of the six parameters, e.g., for $R_1^2$: $a_1 = 0$ and for $R_2^2$: $a_2 = 0$.

## Gimbal Scores

To quantify the twist in the surface fitted to the rotation trajectories, we can compute the gimbal score, $G$, which describes the dependence of the roll component of the rotation vector on the yaw and pitch components of the same vector as follows (12, 16):

$$G = \frac{r_x}{r_y r_z} \tag{9}$$

The roll component ($r_x$) of each trial was plotted against the pitch-yaw product ($r_y r_z$) for conditions NT and PG in Fig. 8. This was done for the same subjects as in Fig. 6.

The gimbal score was then estimated by using linear regression on the plots of $r_x$ versus the product $r_y r_z$, as was done in an earlier study (12). Note that the assumption of a

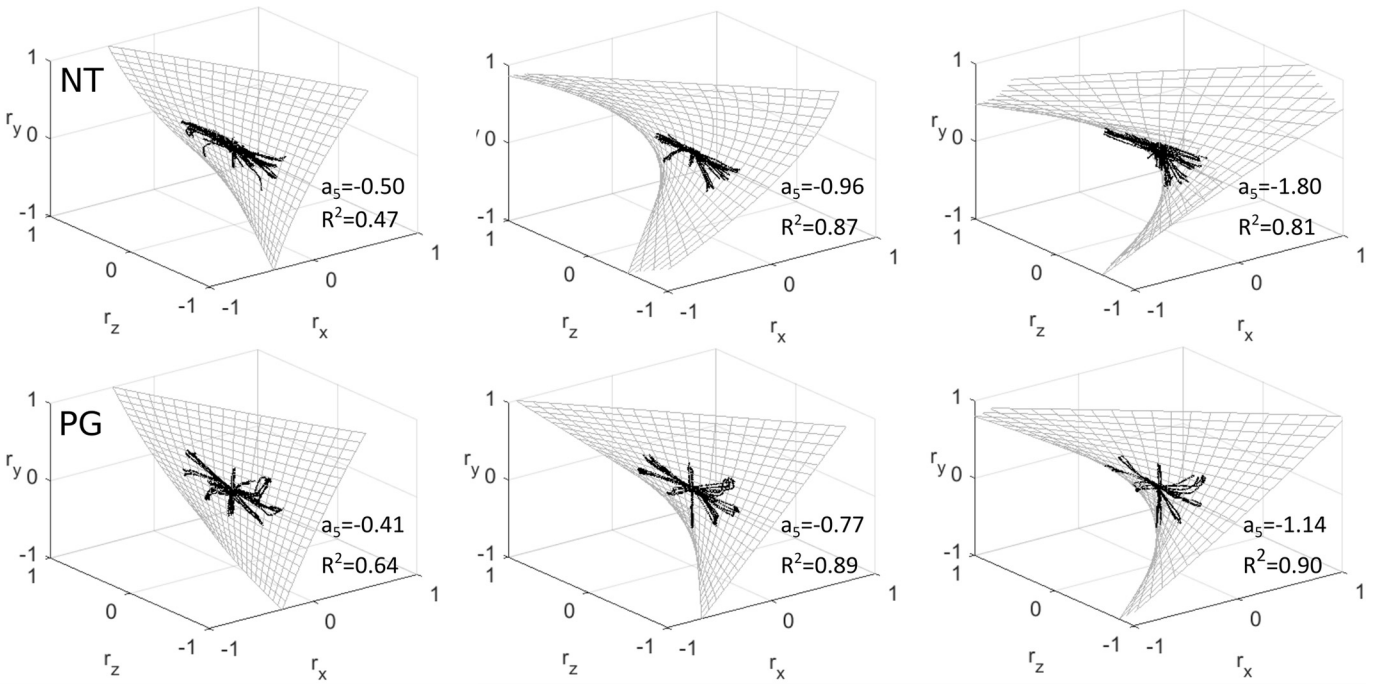


**Figure 6.** Fitted second-order surfaces for subjects with the lowest, median, and highest absolute twist score ($a_5$), respectively, for conditions NT (no torso, *top*) and PG (pinhole goggles, *bottom*). The thick lines are the individual trajectories of the rotation vectors per trial. The respective $a_5$ and $R^2$ values are reported at *bottom right* of each plot.

**Table 1.** *Fitted values for parameter space a of second-order twisted surfaces*

| | NT | PG | Ref. 13 |
|---|---|---|---|
| $a_1$ | 0.000 ± 0.005 | 0.000 ± 0.005 | 0.001 ± 0.002 |
| $a_2$ | −0.019 ± 0.052 | −0.018 ± 0.044 | −0.004 ± 0.024 |
| $a_3$ | −0.003 ± 0.075 | 0.013 ± 0.051 | −0.005 ± 0.064 |
| $a_4$ | −0.105 ± 0.215 | −0.012 ± 0.056 | 0.072 ± 0.071 |
| $a_5$ | −1.062 ± 0.321 | −0.794 ± 0.171 | −0.732 ± 0.268 |
| $a_6$ | −0.017 ± 0.072 | −0.004 ± 0.051 | −0.026 ± 0.064 |

Values are means ± SD computed between subjects. NT, no torso condition; PG, pinhole goggles condition.

linear relationship between $r_x$ and $r_y r_z$ implies that only $a_1$ and $a_5$ affect the twisted surface fit.

Linear regressions were computed for extension and flexion separately, as it was found earlier that positive pitch rotations can lead to different behavior than negative rotations (12). The gimbal score defined in *Eq. 9* was reported for both signs of pitch for easier comparison with previous work.

The mean gimbal scores during extension were close to −1. During flexion, the slopes were somewhat steeper in condition NT and flatter in condition PG (NT extension: −0.988 ± 0.435, NT flexion: −1.217 ± 1.474, PG extension: −0.928 ± 0.358, PG flexion: −0.684 ± 0.254). Note that the standard deviation in NT flexion is very high; the reason for this is discussed in *Roll Is a Linear Function of Pitch and Yaw*.

### *k*-Gimbal Model

We tested five different implementations of the *k*-gimbal model (*Eq. 7*) for prediction of the roll component of the rotation vectors ($r_x$). The first implementation assumed zero roll ($k = 0.5$). The second assumed a truncated Fick gimbal ($k = 0$). Third, we fitted a single $k$ value to the trials combined over all subjects. This led to $k = -0.04$ for NT and $k = 0.10$ for PG. Fourth, a unique $k$ value was fitted for each subject. Finally, a separate $k$ was computed for extension and flexion, leading to two values of $k$ per subject. The $k$ values were obtained by minimizing $r_{x0}$ in *Eq. 7*, using the nonlinear simplex method (fminsearch in MATLAB).

In Fig. 9, we plot, per model approach, the standard deviation (std) of the error between the true and estimated $r_x$ in degrees, also referred to as the torsional thickness σ (13), defined as:

$$\sigma = \mathrm{std}(2 \times \mathrm{atan}(\hat{r}_x - r_x)) \quad (10)$$

where $r_{x0}$ is the amount of roll offset. If $k = 0$, then the model represents a Fick gimbal; if $k = 1$, then it represents a Helmholtz gimbal (see Fig. 2).

Statistical significance between the Fick gimbal ($k_0$) and the other implementations of the *k*-gimbal model was tested with two-tailed *t* tests. Statistical significance was only found for the zero-roll model ($k_{0.5}$) for both conditions NT and PG.

## DISCUSSION

### Rotations Adhere to Donders' Law

The $R^2$ values in Fig. 7 support the notion that head movements generally adhered to Donders' law: in condition NT the mean $R^2$ was 0.80; in condition PG it was 0.85. Furthermore, from the mean values in Table 1 and the $R^2$ values in Fig. 7, we can conclude that the majority of the roll data was explained by the twist score, $a_5$. When $a_1$, $a_2$, $a_4$, or $a_6$ was omitted from the equation, there was almost no effect on $R^2$. The only other factor that appeared to have a small effect was $a_3$, which suggests that there was a small linear relationship between roll and yaw, regardless of the pitch position. This may, however, be a result of the resting head position of some of the subjects. If the zero-pitch orientation of a subject does not properly align the anatomical yaw axis of rotation with the world *z*-axis, then any yaw rotation will inherently have a roll component, resulting again from an $r_y r_z$ interaction. The median thickness scores of 2° in Fig. 9 are in accordance with the scores found in Ref. 16. This suggests that adherence to Donders' law was not influenced by the additional available auditory information in this study.

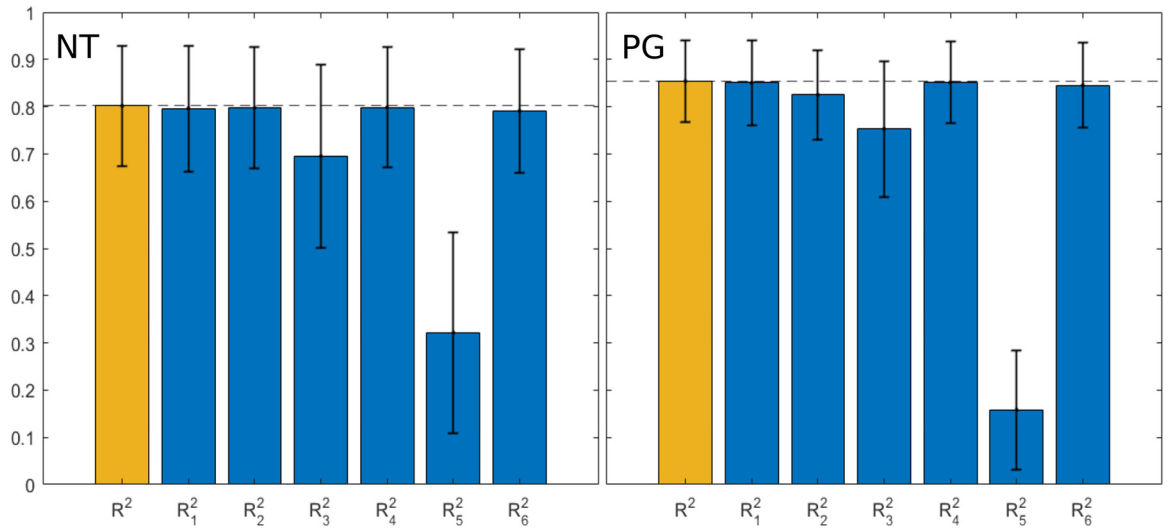


**Figure 7.** Mean and standard deviation of $R^2$ of second-order surfaces fitted to each subject. The yellow bar indicates the $R^2$ value for the twisted surface with all 6 available parameters. The blue bars indicate the $R^2$ value for the surface with 1 parameter excluded, e.g. for $R_1^2$: $a_1 = 0$ and for $R_2^2$: $a_2 = 0$. NT, no torso condition; PG, pinhole goggles condition.

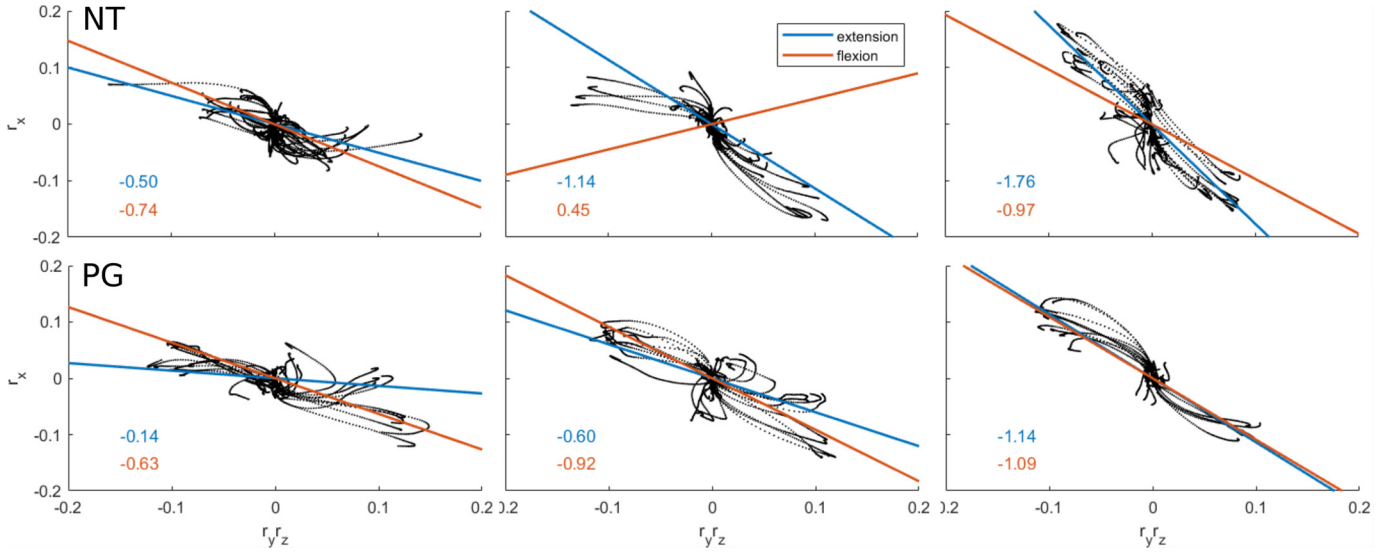


**Figure 8.** Roll component of rotation vector ($r_x$) plotted against the pitch-yaw product ($r_y r_z$) for conditions NT (no torso, *top*) and PG (pinhole goggles, bottom) and for subjects with the lowest, median, and highest absolute twist score ($a_5$), respectively. Linear regressions were computed for extension and flexion separately. The numbers at *bottom left* of each plot indicate the gimbal score *G* from *Eq. 9*.

A standard deviation of 2° is small but may still be significant, given that the upper and lower quadrants of roll were very small (see Fig. 4). For general modeling purposes, however, Donders' law appears to be an appropriate assumption.

### Roll Is a Linear Function of Pitch and Yaw

The high dependence on the twist score, $a_5$, shows that roll was almost strictly a function of the pitch/yaw product. Looking at Fig. 8, we see an almost linear relationship between $r_x$ and $r_y r_z$. We also see that the fitted linear regressions nearly pass through the origin, indicating that the relationship can be modeled as a slope, omitting the offset.

The majority of the gimbal scores (i.e., the slopes of the linear regressions) among all subjects were found to be negative. This supports the characterization of head rotations as a Fick gimbal as opposed to a Helmholtz gimbal (24). There were some exceptions for flexion in condition NT, though the linear regressions in these instances are not very meaningful because of the general lack of flexion performed, as could also be seen in Fig. 4. The sign and magnitudes of the gimbal scores are in general accord with previous studies, which reported values between 0 and −2 (12, 16). Gimbal scores did differ substantially between subjects, which means that there were differences in the amount of roll that they deployed during head rotations.

Interestingly, only a few subjects showed a large difference in slope of the linear regression between extension and flexion, given that the magnitude of flexion was large enough to correctly fit the regression. For those subjects, it does seem necessary to differentiate between two different gimbal models depending on the sign of pitch.

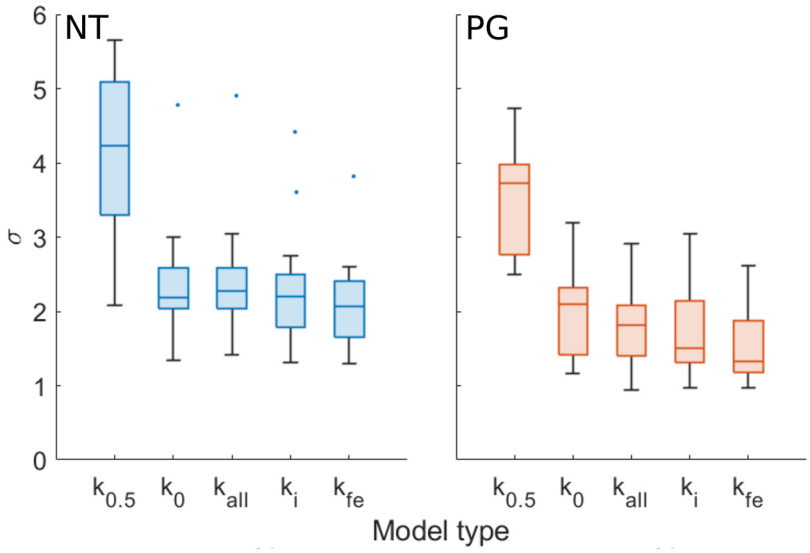


**Figure 9.** Torsional thickness σ (in degrees) of the *k*-gimbal model for 5 different approaches of setting the *k* value. *Left*: NT (no torso condition). *Right*: PG (pinhole goggles condition). $k_{0.5}$: zero roll, $k_0$: Fick gimbal, $k_{all}$: single value fitted to all subjects, $k_i$: *k* value fitted individually for each subject, $k_{fe}$: 2 *k* values fitted for extension and flexion, separately for each individual. Each boxplot shows the statistics of all 17 subjects (median, first and third quartiles, minima and maxima, outliers).

### Rotations Can Be Approximated by a Truncated Fick Gimbal

Different models were tested to include more individualized data. However, Fig. 9 presents the somewhat surprising result that none of the individualization approaches of the *k*-gimbal model significantly improved the model performance. No statistical significance between the different approaches of obtaining the $k$ value means that, although individual differences in the twist score do exist, the truncated Fick gimbal (i.e., $k = 0$) serves as a good approximation for the roll component in the head rotations of the average subject. Thus, the differences in gimbal scores between subjects were not large enough to make full individualization necessary. This is also confirmed by the $k$ values found when fitting over all subjects, which were close to 0 ($k = -0.04$ for NT, $k = 0.10$ for PG). Note that there are a number of subjects where using an individualized $k$ value does improve modeling performance but the majority do not appear to need this.

### Pinhole Goggles Decrease Variability in Rotation

There were some observable differences between the NT and PG conditions. First of all, Fig. 6 and Fig. 7 show that the $a_5$ values were lower in condition PG, whereas the $R^2$ values were higher. This means that pinhole goggles decreased the amount of roll that subjects deployed, while they also made the head movements adhere better to Donders' law. Similarly, it was found earlier that pinhole goggles constrain the head rotation vectors to a plane (i.e., Listing's law) (16). However, the results still could not be well predicted by a planar surface (concluded from the very low $R^2$ score when $a_5$ was omitted in Fig. 7). In Table 1 we also see that the standard deviation of all fitted parameters decreased substantially in condition PG, which means that the pinhole goggles caused the intersubject differences to decrease. One explanation could be that most of the head movement variability between subjects is caused by the extra degrees of freedom from the eyes. Restricting this would then make the subjects behave more consistently. However, the standard deviations in Ref. 13 were similarly small, while the subjects did not have any restricted vision here. Alternatively, the lower standard deviation may be a result of more restricted start and end points, as condition PG forced subjects to fully rotate their heads toward the visual targets (see Fig. 5). In condition NT, any end point that contains the target within the field of view is acceptable. This appears to be a reasonable explanation, as the subjects in Ref. 13 were required to accurately point their head toward each target before moving to the next, which makes the task performed more similar to condition PG. This is further supported by the twist scores of Ref. 13, which are most similar to those of condition PG. Interestingly, the $R^2$ in condition PG is also lower than in condition NT when $a_5$ is omitted. This means that, with pinhole goggles, the twist score describes an even larger percentage of the data. Finally, Fig. 9 shows that thickness scores were consistently lower in condition PG.

### Auditory Cues Keep Head Rotation Behavior Consistent

Because of the restricted vision of condition PG, it was expected that the subjects would depend more on auditory cues to localize the correct target, which in turn might lead to different head movement strategies. From the data collected in conditions NT and PG, this did not appear to be the case, as the trajectories (as seen in Fig. 5) did not differ significantly except for the lower deviation in start and end points, as explained in *Pinhole Goggles Decrease Variability in Rotation*. From this we can conclude that the restricted vision did not fundamentally alter rotation behavior, likely because the available auditory cues kept head movement consistent.

### Limitations

As the aim of the present study was head rotation behavior, we did not extensively investigate head translation. The absolute maximum translations for the $x$-, $y$-, and $z$-axes were substantial (condition NT: 15.4 cm, 9.5 cm, and 4.9 cm; condition PG: 19.3 cm, 10.4 cm, and 8.3 cm; condition F: 20.8 cm, 14.6 cm, and 5.3 cm). It is difficult to infer how much of this translation was due to the definition of the origin of the coordinate system, which was defined slightly above eye level and not on the exact axis of rotation of the head.

A second limitation is that no condition was tested with solely visual information. In the future, it would be interesting to compare rotation behavior to the present study when no auditory information is available.

### Conclusions

In this study, the head movements of 17 subjects were tracked during an auditory-guided visual search task. By fitting a second-order twisted surface to the rotation vectors over all trials, it was shown that Donders' law was generally met, i.e., humans used only two out of three available rotational degrees of freedom. There were intersubject differences in the gimbal score, i.e., the rotation angle around $r_x$ as a function of rotation angles around $r_y$ and $r_z$. Surprisingly, these differences did not lead to a statistically significant improvement when the *k*-gimbal model, which was introduced in previous work (12), was tested with individualized $k$ values. This leads to the conclusion that the measured head rotations could be described by the *k*-gimbal model with $k = 0$. This is equivalent to a truncated Fick gimbal, which consists of a pitch axis nested within a yaw axis. Finally, subjects were more alike in their movements when wearing pinhole goggles. This was likely because the restricted vision enforced clear start and end points of each rotation, resulting in a new set of more consistent, though potentially less natural, head rotations among subjects.

Taken together, subjects generally used similar search strategies following Donders' law to identify an audiovisual target. With restricted vision and therefore an increased dependency on auditory cues, the executed rotations did not change fundamentally. From this we can conclude that visual conditions had little influence on movement behavior because of the available acoustic cues.

Future research might consider the head movements of hearing-impaired individuals, as they have been found to show more unpredictable movement behavior (17, 18). A second avenue for further investigation involves the neural control mechanisms responsible for Donders' law. The fact that head movements follow the same motor rules whether

auditory information is available or not can provide insights into the neural substrates of the control of head movements (33) and of the processing of head motion-related sensory feedback (10).

## DATA AVAILABILITY

Data are available through the function data_mclachlan2024 in the Auditory Modeling Toolbox: https://amtoolbox.org/.

## ACKNOWLEDGMENTS

The authors express their gratitude to Ville Pulkki, who gave approval for the research visit at Aalto University. ChatGPT 3.5 was used for grammatical corrections.

## GRANTS

This research was supported by the Research Foundation Flanders (FWO) under Grant No. G023619N and the Agency for Innovation and Entrepreneurship (VLAIO).

## DISCLOSURES

No conflicts of interest, financial or otherwise, are declared by the authors.

## AUTHOR CONTRIBUTIONS

G.M. conceived and designed research; G.M. and P.L. performed experiments; G.M. analyzed data; G.M. interpreted results of experiments; G.M. prepared figures; G.M. drafted manuscript; G.M., P.L., and H.P. edited and revised manuscript; G.M., P.L., and H.P. approved final version of manuscript.

## REFERENCES

1. **Iwaya Y**, **Suzuki Y**, **Kimura D.** Effects of head movement on front-back error in sound localization. *Acoust Sci Technol* 24: 322–324, 2003. doi:10.1250/ast.24.322.
2. **Kato M**, **Uematsu H**, **Kashino M**, **Hirahara T.** The effect of head motion on the accuracy of sound localization. *Acoust Sci Technol* 24: 315–317, 2003. doi:10.1250/ast.24.315.
3. **McAnally KI**, **Martin RL.** Sound localization with head movement: implications for 3-d audio displays. *Front Neurosci* 8: 210, 2014. doi:10.3389/fnins.2014.00210.
4. **McLachlan G**, **Majdak P**, **Reijniers J**, **Mihocic M**, **Peremans H.** Dynamic spectral cues do not affect human sound localization during small head movements. *Front Neurosci* 17: 1027827, 2023. doi:10.3389/fnins.2023.1027827.
5. **Perrett S**, **Noble W.** The effect of head rotations on vertical plane sound localization. *J Acoust Soc Am* 102: 2325–2332, 1997. doi:10.1121/1.419642.
6. **Thurlow WR**, **Runge PS.** Effect of induced head movements on localization of direction of sounds. *J Acoust Soc Am* 42: 480–488, 1967. doi:10.1121/1.1910604.
7. **Wallach H.** The role of head movements and vestibular and visual cues in sound localization. *J Exp Psychol* 27: 339–368, 1940. doi:10.1037/h0054629.
8. **Carlile S**, **Leung J.** The perception of auditory motion. *Trends Hear* 20: 2331216516644254, 2016. doi:10.1177/2331216516644254.
9. **Lladó P**, **Barumerli R**, **Baumgartner R**, **Majdak P.** Predicting the effect of headphones on the time to localize a target in an auditory-guided visual search task. *Front Virtual Real* 5, 2024. doi:10.3389/frvir.2024.1359987.
10. **McLachlan G**, **Majdak P**, **Reijniers J**, **Peremans H.** Towards modelling active sound localisation based on bayesian inference in a static environment. *Acta Acust* 5: 45, 2021. doi:10.1051/aacus/2021039.
11. **Ghosh BK**, **Wijayasinghe IB.** Dynamics of human head and eye rotations under Donders' constraint. *IEEE Trans Automat Contr* 57: 2478–2489, 2012. doi:10.1109/TAC.2012.2186183.
12. **Kunin M**, **Osaki Y**, **Cohen B**, **Raphan T.** Rotation axes of the head during positioning, head shaking, and locomotion. *J Neurophysiol* 98: 3095–3108, 2007. doi:10.1152/jn.00764.2007.
13. **Medendorp W**, **Melis B**, **Gielen C**, **Gisbergen JV.** Off-centric rotation axes in natural head movements: implications for vestibular reafference and kinematic redundancy. *J Neurophysiol* 79: 2025–2039, 1998. doi:10.1152/jn.1998.79.4.2025.
14. **Zangemeister W**, **Lehman S**, **Stark L.** Simulation of head movement trajectories: model and fit to main sequence. *Biol Cybern* 41: 19–32, 1981. doi:10.1007/BF01836124.
15. **Kim C**, **Mason R**, **Brookes T.** Head movements made by listeners in experimental and real-life listening activities. *J Audio Eng Soc* 61: 425–438, 2013.
16. **Ceylan M**, **Henriques D**, **Tweed D**, **Crawford J.** Task-dependent constraints in motor control: pinhole goggles make the head move like an eye. *J Neurosci* 20: 2719–2730, 2000. doi:10.1523/JNEUROSCI.20-07-02719.2000.
17. **Brimijoin WO**, **McShefferty D**, **Akeroyd MA.** Auditory and visual orienting responses in listeners with and without hearing-impairment. *J Acoust Soc Am* 127: 3678–3688, 2010. doi:10.1121/1.3409488.
18. **Hendrikse MM**, **Eichler T**, **Hohmann V**, **Grimm G.** Self-motion with hearing impairment and (directional) hearing aids. *Trends Hear* 26: 23312165221078707, 2022. doi:10.1177/23312165221078707.
19. **Donders F.** Beitrag zur lehre von den bewegungen des menschlichen auges. In: *Hollandische Beitrage zu den anatomischen und physiologichen Wissenschaffen I*. Dusseldorf: Botticher, 1847, p. 105–145.
20. **Listing JB.** *Beitrag zur physiologischen Optik*. Leipzig: W. Engelmann, 1905.
21. **Von Helmholtz H.** *Handbuch der physiologischen Optik: mit 213 in den Text eingedruckten Holzschnitten und 11 Tafeln*. Leipzig: Voss, 1867.
22. **Haslwanter T.** Mathematics of three-dimensional eye rotations. *Vision Res* 35: 1727–1739, 1995. doi:10.1016/0042-6989(94)00257-m.
23. **Tweed D**, **Vilis T.** Geometric relations of eye position and velocity vectors during saccades. *Vision Res* 30: 111–127, 1990. doi:10.1016/0042-6989(90)90131-4.
24. **Glenn B**, **Vilis T.** Violations of Listing's law after large eye and head gaze shifts. *J Neurophysiol* 68: 309–318, 1992. doi:10.1152/jn.1992.68.1.309.
25. **Radau P**, **Tweed D**, **Vilis T.** Three-dimensional eye, head, and chest orientations after large gaze shifts and the underlying neural strategies. *J Neurophysiol* 72: 2840–2852, 1994. doi:10.1152/jn.1994.72.6.2840.
26. **ANSI/ASA.** *Methods for Measuring the Effect of Head-Worn Devices on Directional Sound Localization in the Horizontal Plane, ANSI/ASA S3.71*, 2019.
27. **Bolia RS**, **D'Angelo WR**, **McKinley RL.** Aurally aided visual search in three-dimensional space. *Hum Factors* 41: 664–669, 1999. doi:10.1518/001872099779656789.
28. **Simpson BD**, **Bolia RS**, **McKinley RL**, **Brungart DS.** The impact of hearing protection on sound localization and orienting behavior. *Hum Factors* 47: 188–198, 2005. doi:10.1518/0018720053653866.
29. **Lladó P, Hyvärinen P, Pulkki V.** The impact of head-worn devices in an auditory-aided visual search task. *J Acoust Soc Am* 155: 2460–2469, 2024. doi:10.1121/10.0025542.
30. **Thurlow WR**, **Mangels JW**, **Runge PS.** Head movements during sound localization. *J Acoust Soc Am* 42: 489–493, 1967. doi:10.1121/1.1910605.
31. **Land MF.** The coordination of rotations of the eyes, head and trunk in saccadic turns produced in natural situations. *Exp Brain Res* 159: 151–160, 2004. doi:10.1007/s00221-004-1951-9.
32. **Zangemeister WH**, **Jones A**, **Stark L.** Dynamics of head movement trajectories: main sequence relationship. *Exp Neurol* 71: 76–91, 1981. doi:10.1016/0014-4886(81)90072-8.
33. **Crawford J**, **Martinez-Trujillo J**, **Klier E.** Neural control of three-dimensional eye and head movements. *Curr Opin Neurobiol* 13: 655–662, 2003. doi:10.1016/j.conb.2003.10.009.